Micromechanical Modeling of Short Crack Nucleation and Growth in High Cycle Fatigue of Martensitic Microstructures

Matti Lindroos[a], Anssi Laukkanen[a], Tom Andersson[a], Joona Vaara[b], Antti Mäntylä[b], Tero Frondelius[c,b]

[a] *VTT Lifecycle Solutions, Espoo, Finland*
[b] *R&D and Engineering, Wärtsilä, P.O.Box 244, 65101 Vaasa, Finland*
[c] *Materials and Mechanical Engineering, University of Oulu, Finland*

Abstract

High cycle fatigue (HCF) is a frequently limiting failure mechanism of machine elements and modern high strength steels. Present day design rules rely on semi-empirical methods, guidelines and utilization of macroscopic analysis means in origin, such as fracture mechanics. The resulting challenge is that short crack regime, critical for HCF in terms of lifetime of components and products, is somewhat poorly handled. This is an outcome of the fact that the present means and methodologies do not explicitly account for effects arising from material microstructure, an oversight micromechanics aims to rectify.

Micromechanical modeling operating on fatigue at the scale of material microstructure necessitates the introduction of suitable means to describe the mechanisms of cyclic plastic deformation and microstructural morphologies, considered critical for HCF especially at the early stages of micro-crack nucleation and damage evolution towards and within the short crack regime. In current work, a crystal plasticity based approach with combined hardening is utilized to capture the respective deformation response utilizing full field modeling. The modeling is carried out for both simplified prior austenite grain like microstructures as well as complex imaging based martensitic quenched and tempered steel microstructural models. A fully coupled damage modeling scheme is introduced to track damage nucleation and evolution at the scale of the studied microstructures. Crack closure is included within the approach to track behavior of microstructure scale defects under, e.g., fully reversed loading, more realistically. Model calibration is addressed and

application cases involving damage and crack growth both under monotonic and cyclic loading are presented.

The results demonstrate how the coupling of damage to crystal plasticity modeling can be utilized to identify and track the evolution of microstructure scale damage mechanisms in complex martensitic microstructures. Interactions between strain localization and damage accumulation are presented as well as transition from micro-cracking to short crack growth. The results show that the proposed approach can interpret the intricate dependencies and relations between complex microstructures, their (cyclic) deformation mechanisms and evolution of damage, the outcomes regarding crack formation and behavior are found to be in line with similar experimental studies.

The proposed framework for modeling damage in polycrystalline microstructures is quite general in its capabilities. By solely introducing a suitable crystal plasticity based deformation model and a damage model describing nucleation and softening can plastic slip and damage interactions be studied in complex microstructures, and in principle, on any system where similar constitutive models are utilizable. The exploitation of the resulting micromechanical modeling and simulation capabilities lies both in simulation driven design of fatigue resistant components and high strength steels.

Keywords: High Cycle Fatigue, Crystal Plasticity, Micromechanics, High Strength Steel

1. Introduction

High cycle fatigue (HCF) is often a limiting failure mechanism when it comes to structural and mechanical machine elements [1, 2]. Studies on HCF have indicated that the role of microstructural defects and initation sites for microstructurally short fatigue cracks dominate the respective loading cycles to failure, i.e., most of the fatigue life is spent while the defect is of microstructure scale and smaller than some respective characteristic material dimension, such as prior austenite grain size (PAG). As such it comes as no suprise that ever more emphasis is being placed on understanding, and particularly, quantitatively modeling, the interactions between the microstructure, different microstructural defects, and nonmetallic inclusions in modern high strength steels.

The present state-of-the-art as far as evaluation of HCF affiliated material properties and design guidelines is largely presented by Murakami and

Endo [3] who performed a thorough review of fatigue assessment methods for fatigue failures initiating from non-metallic inclusions. Their method to predict fatigue strength has gained momentum and is described by the following points [4]:

- Short fatigue cracks threshold stress intensity factor range depends on the inclusion size with logarithmic slope of 1/3
- Short fatigue crack threshold depends linearly on the matrix hardness (up to 720 HV)
- Inclusions behave similarly in fatigue as holes produced by focused ion beam or drilling
- Fracture mechanics based size indicator of projected $\sqrt{area}$ of the inclusion in the direction of the maximum principal stress characterizes the maximum stress intensity factor of many differently shaped cracks (aspect ratio $a/b < 5$)

The developments in crystal plasticity modeling of cyclic plastic slip response at the scale of the material microstructure have led to ever increasing number of studies attempting to establishing relations between plastic slip, stress triaxiality and fatigue failure mechanisms. The resulting micromechanical models have approached the topic in two principally different ways: firstly, by defining oftentimes cycle specific Fatigue Indicator Parameters (FIPs), and, secondly, by direct approaches where material microstructure scale plastic slip and stress state are utilized to assess material damage due to cyclic loading. With respect to such efforts, Sangid et al. [5, 6, 7] used persistent slip band's energy instability in conjunction with dislocation creation in micromechanical configuration to predict fatigue life scatter for U720. Pineau and Forest [8] performed elastic-plastic finite element calculations to assess the role of cyclic plasticity and residual stresses for very high cycle fatigue (VHCF) at the matrix-inclusion interface. Proudhon et al. [9] performed a 3D simulation of short fatigue crack propagation incorporating finite elements, crystal plasticity and remeshing. This is one of the few works which considers damage evolution beyond FIP like parameters but also models short fatigue crack propagation, albeit in a simplistic setting. Frondelius et al. [1, 10] studied inclusion to microstructure interactions in a high strength steel to develop micromechanical analysis methods for assessing the influence of defect structures to nucleation and short crack regime damage evolution in the HCF region. In Li et al. [11] the cyclic behaviour at the sub-grain level was predicted and the effects of lath and precipitate sizes examined for elevated temperature response of respective steels. A crystallographic, accumulated slip (strain) parameter, modulated by triaxiality, was implemented at the micro-scale in order to predict crack initiation in precipitate-strengthened laths. In [12] Guan et al. replicated single and oligocrystal microstructures and their deformation behavior with crystal plasticity finite element models and under fatigue loading performed analyses that enabled grain-by-grain comparison of measured and calculated slip to be carried out. Single and multiple slip activation, slip localization and microstructure-sensitive stress evolution were examined. The initiation of slip in the single crystals was found to be highly localized in bands, of about 1–2 μm thickness and 30 μm separation. With increasing loading, the bands thickened to develop a more uniform field of straining, these features of deformation behavior were captured with crystal plasticity modelling. Bribier et al. [13] performed crystal plasticity analysis on Ti-6Al-4V under high cycle fatigue. Their model employed softening model related to dislocation slip that eventually triggers fatigue. A simplified 3D microstrucure was used to analyze performance of the microstructure aiming to capture damage nucleation and growth in two phase microstructure.

For some materials, physically material short cracks have been found to initiate easily and the fatigue limit is defined by retardation of the growth of these cracks [4]. The near-threshold crack growth behaviour emphasizes roughness- and oxide-induced crack closure [14]. Much of the experimental work studying crack closure has been focused on positive stress ratios. Pommier et al. [15] and Silva [16, 17] found that for crack closure under negative stress ratios the role of material's cyclic plastic properties, and especially kinematic hardening, is emphasized and a clear dependence on the stress amplitude was found. The levels of crack closure approached those of zero stress ratio near threshold as cyclic plasticity is suppressed [15]. Development of crack closure is also emphasized with cracks growing from notches and could be important in the case of cracks initiating from non-metallic inclusions. See Vaara et al. [18] for a brief review on high-cycle fatigue with focus on non-metallic inclusions and forming. In any event, due to the anisotropy and complex microstructural morphologies at the scale of the material microstructure, it is envisioned that particular emphasis needs to be placed on the capability to consider microstructure scale crack closure associated behavior.

Next generation fatigue design methodologies aim to utilize micromechanics at their core. The impact being sought is improved accuracy to be able to avoid unexpected failures and improve power density of products and components while doing so. Also, steps toward virtual testing of materials are to be expected. Simultaneously, if microstructure scale phenomena dominating fatigue life can be accurately modeled, it opens up the possibility to virtually design novel materials and optimize material solutions. For defect critical failure mechanisms such as HCF, this will make it possible to systematically develop the microstructures and manufacturing processes to target performances and functionality profiles of specific products.

The focus on current study is in developing and demonstrating fully microstructure and deformation coupled damage mechanical models for micromechanical evaluation of fatigue, that is applicable also to HCF. Rather than utilize, e.g., FIP parameters to correlate to cyclic fatigue damage, a direct fully crystal plasticity coupled approach is adopted. The constitutive model is applied for different complexity containing models of martensitic microstructure, typical to those of quench and temper (Q&T) steels. A "smeared" approach tracking crack closure is integrated in the model to include the effects of crack face contact. The material model is calibrated for a Q&T-steel based on digital image correlation (DIC) instrumented tensile tests. As use cases deformation and damage evolution under monotonic and cyclic loadings is investigated and compared to, e.g., typical crack propagation behavior and trajectories in martensitic microstructures. The demonstrative results provide a basis for utilizing micromechanical modeling to directly infer and investigate damage accumulation in complex microstructures related to HCF of high strength steels.

2. Materials and methods

2.1. Material

Wrought Q&T steel of 34CrNiMo6 grade with a nominal tensile strength of 1025 MPa and a nano-hardness of 4.7 $\pm$ 0.3 GPa is studied in this work. The steel grade can be used in applications requiring decent strength and ductility combined with a good resistance to fatigue, for example such as in engine components. SEM (Scanning Electron Microscopy) with EBSD (Electron Backscatter Diffraction) detector was used to characterize the microstructure of the material which is shown in Figure 1a. Conventional sample preparation techniques was used and the sample was polished prior to

SEM and EBSD measurements. The microstructure is lath martensitic. Depending on the material's manufacturer and process specifics, different defects may exist in the material. The material can include different individual inclusions and clusters of inclusions (typically, e.g., alumina) infused with other slag components. Current work focuses on the modeling of plasticity and damage in Q&T steel microstructure, and therefore the effect of local defects is omitted from the present scope. Thus, the material is assumed ideally coherent martensite, as is apparent in Figure 1.

2.2. Computational microstructures

To investigate the deformation and damage behavior of the material, two polycrystalline microstructures were chosen for the study. The first phase of the simulations involves a tesselated representative volume element (RVE) that is shown in Figure 1b. It includes a typical prior austenite grain structure with 100 grains all assigned to different orientations. The microstructure is used for crystal plasticity model parameter identification in Section 3.2 to capture polycrystalline effects with arbitrarily shaped grains and grain boundaries, which can affect crack/damage evolution. The same simplified microstructure RVE was utilized also in the simulation of cyclic loading conditions in Section 3.4. A more detailed and relevant QT microstructure in Figure 1c representing lath martensite was extracted as a computationally efficient subset from the large EBSD scan in 1a. The finite element mesh was based on the EBSD imaging of the microstructure segmented based on a presumed discrete orientation distribution capturing the misorientation relationships as common in martensite. The finite element meshes and models were obtained using methodologies described in more detail in [19, 20, 21]. Advanced characterization techniques exist to track crack growth in 3D [22], which could provide more detailed information for the material identification. However, the present work focuses on the demonstration of the modeling framework.

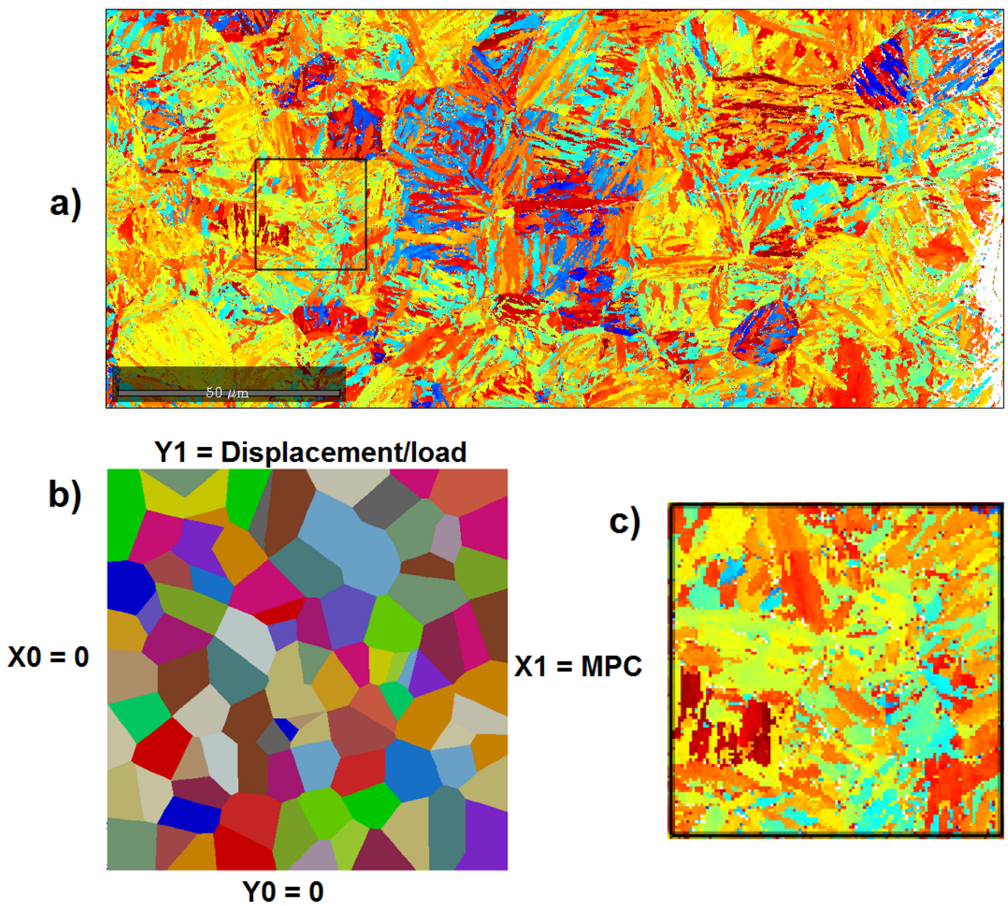

Figure 1: a) Scanning electron microscope image with a orientation map of the Q&T-steel, b) polycrystalline microstructure and c) substracted computational martensitic microstructure used in the simulations.

The computational domains were constrained to retain uniform deformation at the boundaries (kinematic uniform boundary conditions). The RVEs were constrained by a direct displacement boundary condition at one side of the RVE and by a multipoint displacement constraint at the other side. Displacement controlled loading was applied throughout this work.

2.3. Experimental setup

In order to analyze the strain hardening/softening behavior of the Q&T steel (forged, quenched and tempered), a uniaxial tensile test program with frequent unloadings to investigate accumulation of damage was established. The aim of the test sequence is to increase the strain of the sample in increments up to failure and record the decrease in elastic modulus, the "effective damage" in a scalar valued form. Approximately one percent increments in strain were used by first loading the material and then unloading it to almost zero load, before following with next loading increment. The test was strain controlled up to two percent of strain and displacement controlled thereafter with a rate of 1.5 percent per minute. The loading and unloading rate was carried out at approximately 20 MPa per second and a minimum threshold of 10 MPa was used at the end of unloading phase.

An attempt to evaluate effect of coupled plasticity and damage from the experiments and to support model parameterization was performed. Besides only obtaining tensile stress-strain curves with a failure point, the degradation of elasticity could be approximated from the unloading curves as a function of macroscopic strain. Hence, a classical Lemaitre-type of damage effect of the elasticity of metals is sought-after in the experiments and therefore we denote this experimental procedure as Lemaitre-type tensile test in the present context (see Lemaitre [23] for background). A 50 mm extensometer was used to measure full length deformation of the samples with 12.5 mm range. In addition, DIC system was used to analyze local deformation. A DIC framerate of 2 Hz was chosen. The sample size was 10 mm in diameter. A spatial resolution of 21.5 pixels per millimeter was chosen. The speckle size pattern was considered rather macroscopic with 5-20 pixels. Hence, the DIC system was employed to measure the in-situ diameter of the test samples. The data was used to correlate between engineering stress and apparent true stress of the samples by correcting the cross-sectional data during deformation.

It is noteworthy that the error of the technique increases towards higher localization as the cross-sectional area of the tensile bar does not necessarily retain its symmetricity, which can cause uncertainties at the end of the test curve. In spite of this typical possibility, the cross-section of the samples were assumed circular throughout the engineering to true stress correction procedure and provide data the very least from the early stages of necking that can be considered valid. Both engineering stress data and corrected true stress data were used in the comparison between experiments and simulations.

2.4. Crystal plasticity model

The crystal plasticity model is extended to couple single crystal plasticity and micromechanical description of damage, inspired by studies focusing on this direct formulation [24, 25, 26]. The following single crystal model was implemented in Zset-software and it as used for finite element simulations in this work. Deformation gradient is decomposed into elastic and inelastic parts:

$$\underline{F} = \underline{F}^{e} \cdot \underline{F}^{in} \tag{1}$$

Inelastic deformation gradient $\underline{F}^{in}$ features both plastic deformation and damage contribution. In the present model, a concept of inelastic damage strain is adopted [24, 25], to distinct contributions of plasticity and damage in single crystal formulation. It also follows that inelastic strain rate $\underline{\dot{F}} \cdot \underline{\dot{F}}^{-1}$ is not always traceless because occurrence of volume change that is associated with damage.

$$\underline{\dot{\epsilon}}^{in} = \underline{\dot{\epsilon}}^{p} + \underline{\dot{\epsilon}}^{d} \tag{2}$$

The model has three important features. Firstly, this approach allows for the damage to operate on crystallographic planes and to produce damage strain according to specific assigned mechanism, i.e., cleavage damage strain operating on the cleavage planes of the single crystals. The formulation also quantifies that damage is not exactly bounded to be a variable between zero and one in contrast to conventional continuum damage approaches. Secondly, more recent development of similar strain based single crystal damage model [25] demonstrated that besides the model describes damage evolution and related material softening, it also aims to describe crack closure. Thirdly, the model features a two-way coupling between damage and plasticity, which means that damage allows plastic localization and on the other hand plastic localization makes it easier to nucleate and grow damage (cracks).

The plastic deformation of the polycrystalline material, without any damage, is described with a rate dependent crystal plasticity model. Dislocation slip is considered to carry out plasticity in martensitic steels. The slip rate is described by phenomenological slip rate formulation.

$$\dot{\gamma}^s = \dot{\nu}\ sign(\tau^s) = \left\langle \frac{|\tau^s - x^s| - r^s - \tau_0}{K} \right\rangle^n sign(\tau^s - x^s) \tag{3}$$

where material parameters K and n characterize the viscosity, τ^s is the current resolved shear stress in a system s, τ_0 is the initial shear resistance of slip system families $\{110\} < 111 >$ and $\{112\} < 111 >$, and r^s is the isotropic hardening variable. For simplicity, the slip resistance is assumed the same for both slip families. The resolved shear stress is computed utilizing the Mandel stress $\underline{M}$ in the intermediate configuration, so that:

$$\tau^s = \underline{M} : \underline{m}^s = (\underline{C}^e \cdot \underline{S}^e) : \underline{m}^s = (\underline{C}^e \cdot (\underline{\underline{\Lambda}} : \underline{E}_{gl})) : \underline{m}^s \tag{4}$$

where $\underline{C}^e$ is the Cauchy-Green tensor, $\underline{E}_{gl}$ is the Green-Lagrange strain tensor, and $\underline{\underline{\Lambda}}$ is the elastic stiffness tensor, and . The second Piola-Kirchhoff stress tensor $\underline{S}^e$ and the Mandel stress tensor $\underline{M}$ are connected in the usual manner by $\underline{M} = \underline{C}^e \cdot \underline{S}^e = (\underline{F}_e^T \cdot \underline{F}_e) \cdot (\underline{\underline{\Lambda}} : \underline{E}_{gl})$, where $\underline{F}_e$ is the elastic part of the deformation gradient.

The evolution of the kinematic hardening parameter x^s is computed with the following evolution equation.

$$x^s = c\alpha_s \ ; \ \dot{\alpha}_s = (sign(\tau^s - x^s) - d\alpha^s)\dot{\nu}^s \ ; \ \nu^s = \int_0^t |\dot{\gamma}^s| \tag{5}$$

where the rate of cumulative plastic slip $\dot{\nu}^s$ controls the evolution of the kinematic hardening, and coefficients c and d are related to its intensity.

Both of the included slip families $\{110\} < 111 >$ and $\{112\} < 111 >$ share the same flow rule. However, the viscous parameters K and n can be different in addition to dissimilar critical resolved shear stresses for the activation, if necessary, and the parameters can be identified from the experimental data and characterization if such are available. All of the slip systems in a slip family are assumed to have the same critical value for activation for simplicity.

Sabnis et al. [25] suggested a coupling between plasticity and damage, in which damage is driven by plasticity. Accordingly, apart from conventional treatments of hardening formulations, we consider that strain accumulation decreases the local cleavage resistance, and thus producing a link between plastic deformation and susceptibility to damage. Free energy density function is formulated to consist elastic, plastic and damage contributions, respectively.

$$\rho\Psi(\underline{\epsilon}^e, \nu, d) = \rho\Psi^e(\underline{\epsilon}^e) + \rho\Psi^p(\nu) + \rho\Psi^d(\nu, d) \tag{6}$$

The additional contribution of damage in the free energy potential contribution takes a form:

$$\rho\Psi^d = Y_0 d + \frac{H}{2}(d + \beta\nu)^2 \tag{7}$$

where Y_0 is the initial cleavage resistance, described in detail below. H is a softening parameter and β plasticity-damage coupling parameter, and d is the cumulative damage, the rate of which is defined by crack opening and two shear mechanisms as:

$$\dot{d} = \sum_{s=1}^{N_{damage}} |\dot{\delta}_c^s| + |\dot{\delta}_1^s| + |\dot{\delta}_2^s| \tag{8}$$

Isotropic hardening is produced for all systems, including contributions from self and latent hardening. The present expression, in Equation 9, considers the interactions between the two slip families. The coupling between plasticity and damage relates isotropic hardening and softening arising from the contribution of damage, which is obtained by partial derivation of the free energy functional:

$$r^s = \rho\frac{\partial\Psi}{\partial\nu} = \tau_0 + Q\sum_r H_{rs}\{1 - exp(-bv^r)\} + H\beta^2\nu + H\beta d \tag{9}$$

The effect of damage does not diminish even if the crack becomes closed, i.e., crack opening strain is zero, because plastic softening coming from damage is controlled by cumulative damage form presented in Equation 8. A case where high damage strains can introduce excessive softening in the crack closed state can realize after severe plasticity and damage. Therefore regularization of damage softening may be required that simply saturates the damage softening contribution to a maximum softening value. In general, the softening-coupling modulus H describes the softening effect of micro-cracking in the material, which accelerates both damage and plasticity.

The interaction matrix H_{rs} is adopted from the work of Hoc and Forest [27] on a BCC material. The form of the interaction matrix showed good

Table 1: The coefficients for the interaction matrix in BCC crystals

Plane	$\{110\} \cap \{110\}$	$\{110\} \cap \{112\}$	$\{112\} \cap \{112\}$
Same	a_0 (h_8)		$k_{s0}a_0$ (h_1)
Collinear	k_1a_0 (h_2)	$k_{p1}a_0$ (h_3)	$k_{s0}k_1a_0$ (h_6)
No collinearity	$k_2k_1a_0$ (h_4)	$k_{p2}k_{p1}a_0$ (h_5)	$k_{s0}k_2k_1a_0$ (h_7)

agreement with experiments involving complex loading paths that may occur in loading various loading conditions including multi-axial fatigue. The number of independent coefficients is reduced to eight within the 24x24 interaction matrix, i.e., classifying the slip systems belonging to the same slip family, to a collinear system or to a non-collinear system. These interactions are presented in Table 1. Kinematic hardening parameterization is obtained from earlier cyclic tensile tests, while calibration of the isotropic response is describe in detail within the results section.

We retain the assumption that interaction between planes $\{110\}$ is smaller than between planes $\{112\}$ [27].

The rate of damage process (crack growth) includes crack opening rate and modes II/III crack shearing rates on all given cleavage planes:

$$\underset{\sim}{\dot{\epsilon}}^d = \sum_{s=1}^{N_{damage}} \dot{\delta}_c^s \underline{n}_d^s \otimes \underline{n}_d^s + \dot{\delta}_1^s \underline{n}_d^s \otimes \underline{l}_{d1}^s + \dot{\delta}_2^s \underline{n}_d^s \otimes \underline{l}_{d2}^s \tag{10}$$

where $\dot{\delta}_c^s$, $\dot{\delta}_1^s$, $\dot{\delta}_2^s$ are the strain rates for mode I, mode II, and mode III crack growth, respectively. N_{damage} denotes the number of damage planes, which are fixed crystallographic cleavage planes for given crystal structure. Cleavage damage is represented by the opening δ_c of crystallographic cleavage planes with the normal vector $\underline{n}^s$ and other damage systems must be introduced for the in-plane accommodation along orthogonal directions $\underline{l}_{d1}^s$ and $\underline{l}_{d2}^s$ once cleavage opening has initiated. The model considers the BCC cleavage planes of type $\{100\}$ for martensitic steels, which have been experimentally observed to have significant effect in the crack initiation and propagation for martensitic and ferritic steels [28, 29]. The evolution of the opening rate is given by:

$$\dot{\delta}_c^s = \langle \frac{|\sigma_{dc}| - Y_c^s}{K_d} \rangle^{n_d} sign(\tau_{dc}) \quad with \quad \sigma_{dc} = \underline{n}_d^s \cdot \underset{\sim}{M} \cdot \underline{n}_d^s \tag{11}$$

The opening rate $\dot{\delta}^s_c$ is driven by the normal component acting on cleavage planes whenever normal stress σ_{dc} exceeds the cleavage crack resistance Y^s_c. Initially only positive stress σ_{dc} can initiate cleavage. After crack opening, the crack is allowed to close if the opening stress is negative with a constraint that $\delta^s_c \geq 0$, which renders a crack closure scheme possible for the model.

The rate of Mode II and III shear mechanisms operating in conjunction with cleavage crack opening mode I are given by a similar rate dependent formulation:

$$\dot{\delta}^s_{1,2} = \langle \frac{|\tau_{di}| - Y^s_i}{K_d} \rangle^{n_d} sign(\tau_{di}) \quad with \quad \tau_{di} = \underline{n}^s_d \cdot \underline{M} \cdot \underline{l}^s_{di} \tag{12}$$

where shear stress τ_{di} drives the damage shear mechanisms when shear resistance Y^s_i is overcome. In both crack opening and shearing mechanisms, K_d and n_d are viscous parameters.

The damage resistance of the material consists material's initial cleavage resistance Y_0 that can vary within the microstructure depending on the defect population and other nanostructural material characteristics. The initial resistance can be different for crack opening and shear mechanisms, but it is assumed to be the same in the present context. Obtaining a partial derivative with respect to damage of the free energy function yields opening/shear resistance for cleavage:

$$Y = \rho \frac{\partial \Psi}{\partial d} = Y_0 + Hd + H\beta\nu \tag{13}$$

Cumulative damage d has direct softening effect on the residual cleavage resistance, while plastic localization softens the material via coupling factor β. It is worth noting that the final cleavage resistance is not exactly zero because of viscous components arising from visco-plastic and visco-damage formulation via parameters K and n as well as residual component of cleavage resistance can be assigned to improve convergence.

A difference exists between previous developments of this type of damage framework in small deformations [24, 25]. The present model omits micromorphic damage regularization in the formulation to drastically decrease overhead of the computations of large microstructures in the absence of new degree(s) of freedom and complexity of the microdamage concept, when finite strains are considered. This simplification makes the damage zones more diffuse in the present model and somewhat mesh size dependent in terms of damage width, which is inherent characteristics of finite elements. A better description of mesh-independent damage is achievable by introducing damage size dependent regularization.

3. Results

3.1. Deformation and damage response

The model response is demonstrated in cyclic uniaxial test in Figure 2 performed on a single element and single crystal case with a displacement control loading, demonstrating also the behavior of the smeared contact approach. The material is first loaded in tensile direction to cause severe plasticity and strain hardening, and then reversed to compression to further allow plasticity to develop. This cycle decreases the cleavage resistance of the material through damage-plasticity coupling and reversion back to tension shows initiation of cleavage. The crack opening occurs and the material quickly softens further promoting crack opening. The loading is again reversed to compression and crack closure begins with diminishing stress resistance until crack opening strain reaches zero and crack is considered closed. At this point, the material regains some of its original strength, which itself is degraded according to Equation 9. Finally if the loading is reversed to tension, the material has very small resistance against cleavage when being already highly damaged and the crack opens with ease.

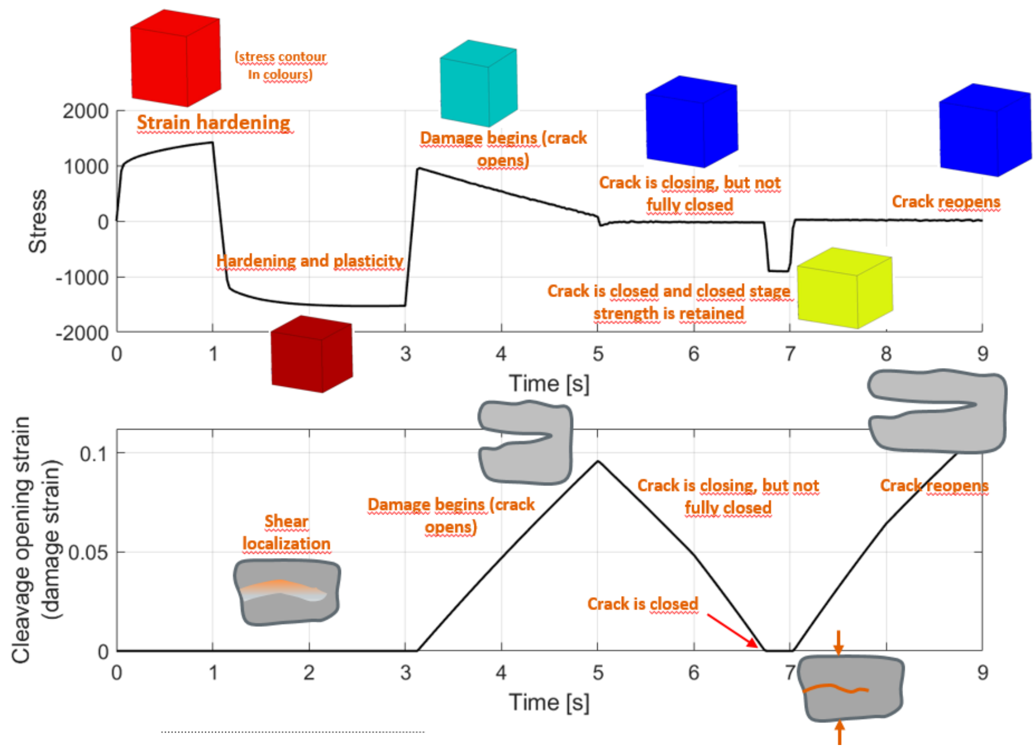

Figure 2: Plasticity-damage model response and crack opening-closure behavior. Element colors describe stress intensity with red being high stress and blue zero stress.

3.2. Damage model parameterization

The stress-strain response of the constitutive model is affected by the coupling between plasticity and damage, which means that hardening part of the stress-strain curve is greatly influenced by the softening and coupling parameterization of the model. Therefore the following presents some cases where damage softening and coupling parameterization is altered, while dislocation slip hardening parameters were kept constant. Figure 3 shows the effect of softening parameter H to the stress-strain and damage responses during an uniaxial tensile test. A polycrystal microstructure with 100 grains as presented in Figure 1 was used in the analyses. The stress-strain, damage and equivalent plastic strain values were obtained by averaging over the whole computational microstructure domain. Low softening modulus value retards the occurrence of damage to relatively high strains and hardening of the material prevails with this parametrization. High softening values, such as -3000 MPa, accelerate the degradation of material strength and cleavage resistance, leading to early damage initiation and spontaneous spreading of the damage. The growth rate ($\partial d/\partial \epsilon$) of damage can be controlled also with the softening modulus, which is evident when comparing the -3000 MPa and -1750 MPa cases. The coupling parameter was kept constant at 0.265 during the simulations.

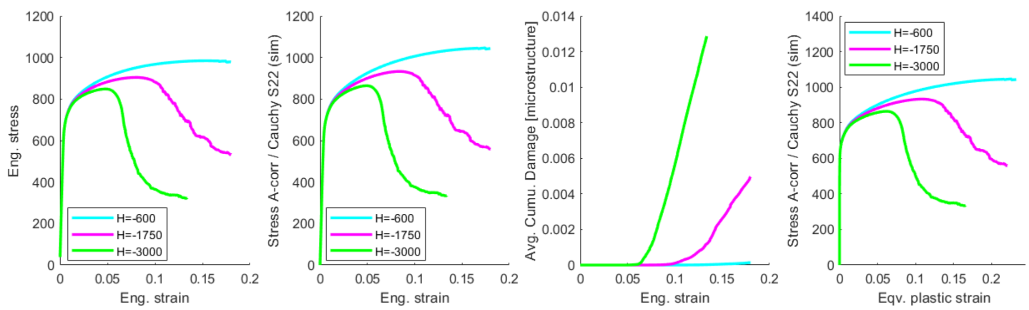

Figure 3: Effect of material softening to stress-strain-damage response

The coupling parameter has similar retarding or accelerating effect to the damage initiation as well as on the softening of stress-strain response. The effect of coupling factor is shown in Figure 4. The softening parameter was kept constant at -1750 MPa during the simulations. A physical interpretation of softening parameter could be considered as a ductility parameter which represents material's capability to continue plastic deformation even at high localization strains and in the presence of damage, while it also has great influence on the effective rate how rapidly damage (cracking) occurs. The coupling parameter then is a similar measure of how easily and quickly existing damage leads to further plastic strain localization and on the other hand what is the contribution of localized plastic strain to damage nucleation and growth processes.

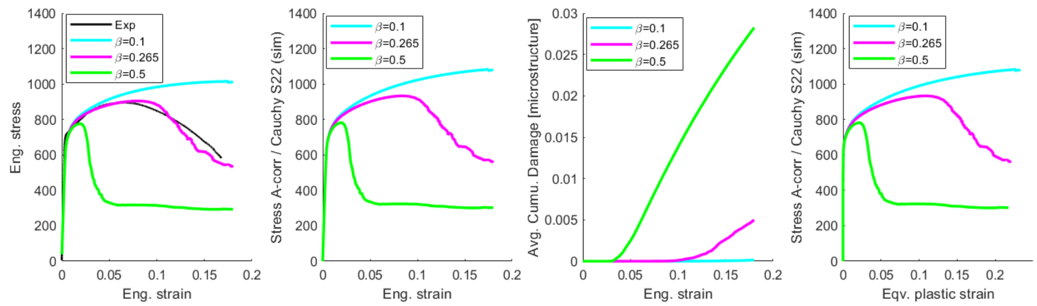

Figure 4: Effect of damage-plasticity coupling.

In both of the previous sensitivity analysis cases, it is clear that the balance between each parameter and their effect on stress-strain response is not straightforwardly identifiable. A principal assumption is made that coupling parameter would lie in the moderate region, e.g., 0.2-0.4. Larger values would lead to very early damage initiation and material would experience brittle like behavior, which would be more typical for untempered martensite. Low values favor plasticity driven damage process, where extensive strain localization would be required, making it more suitable for ductile materials. A follow up to current work is to further investigate the dependencies utilizing molecular and dislocation dynamics modeling as well as in-situ microstructure resolution tensile testing. Although these methodologies have challenges with respect to spatial and temporal scales with respect to modeling polycrystals, they are still foreseen to yield additional data to support solely experimentally driven calibration approaches.

Figure 5 compares the Lemaitre-type of uniaxial tensile loading-unloading experimental results with the simulated response of the model. Figure 5a shows the engineering values. Figure 5b shows an expression of true stress state against engineering strain. The true stress for experiments was obtained by correcting engineering stress with the instantaneous cross-sectional area that was defined as equivalent area in the necking region by measuring the diameter of the tensile bar with DIC system in the two dimensional analysis, as explained in Section 2.3. The corrected experimental true stress values were thus compared against an axial component of the Cauchy stress tensor of the simulations, which is the stress component in the loading direction. The results have good agreement throughout the strain range. The damage dominated region beyond 0.1 of strain shows largest difference because of the uncertainties related to damage evolution of the material as well as in the definition of the cross-sectional area used to compute the experimental true stress. Furthermore, it is also evident that the material's softening behavior is not constant in the three experimental cases and the scatter is relatively large when compared to the more constant hardening part of the stress-strain curve. A parametric simulation study revealed that it is possible to adjust the shape of the curve in the damage dominated region by varying the softening and coupling parameters ($\pm$ 200 MPa, and $\pm$ 0.02, respectively). Yet, given experimentally observed scatter the parameterization can be considered acceptable due to the results residing within the experimentally observed scatter. Figure 5c shows the true stress as a function of inelastic strain. The inelastic strain was defined as the plastic part of total strain measured during the experiment, i.e., total strain comprises elastic and inelastic strain contributions. No direct distinction between plasticity and damage could be made in the experiments. The value from simulations corresponds to the average of inelastic strain over the microstructure. The actual local strains are much larger than the average strain of the sample, which explains the difference between the experiment and simulations.

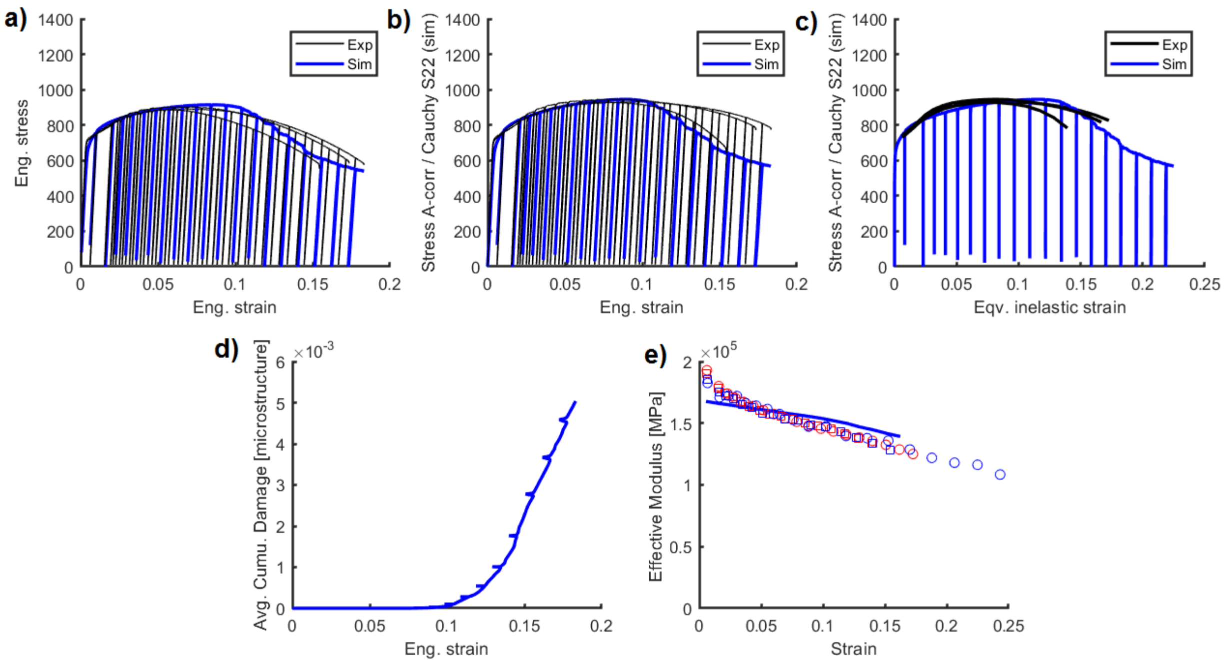

Figure 5: Experimental loading-unloading tensile experiment used for model parameter fitting. a) Engineering stress and engineering strain, b) simulated true axial stress and experiment based area corrected stress c) true stress and inelastic strain (simulated and exp. extensometer), d) cumulative damage over the RVE micrsotructure, e) effective elasticity measured from unloading curves of experiments (extensometer and DIC) and simulations.

The elastic stiffness of the material is not explicitly degraded in the model by bounding damage variable to instantaneous elastic moduli as a function of microcracking. It is assumed that plasticity dominates over elasticity during hardening and also during the rapidly developing cracking process. One fundamental aim of the Lemaitre-type damage experiment is to approximate the change in the effective stiffness of the material, i.e., damage degrading the elasticity of the material. In the experiments, the effective elastic modulus was determined from the unloading curves after each loading increment using extensometer data and DIC measurements. Figure 5d shows the accumulation of damage in the microstructure as a function of cumulatively increasing strain during the loading-unloading sequence. Once damage is initiated, its effect quickly increases. During unloading, cumulative damage increases slightly when the cracks start to close under compression. Figure

5e plots the degradation of elasticity as a function of equivalent inelastic strain. It can be seen that the material experiences notable loss of stiffness when inelastic strain increases. The simulation model can correlate similar degradation in elasticity to a certain degree, but because of lacking full coupling between damage and elastic moduli, a deviation in the results is to be expected. Simulations showed that damage itself can largely accurately account for the loss of stiffness, but in such cases the hardening of the material must to be set to unrealistic low.

Figure 5e shows the evolution of damage during the simulation range. The shape of the curve shows that the repeated loading sequences first initiate and grow damage slowly, i.e., interpretable as small microcrack growth dominated region in the damage process. Figure 6a visualizes total inelastic strain contributed by plasticity and damage at 8 % of macroscopic strain. After the initiation, the rate of damage and associated plasticity rapidly increase between 0.11 and 0.18 of macroscopic strain. Figure 6b,c. shows these two stages of inelastic strain localization. Damage and plasticity continues to localize between two nucleation sites, which both are in the vicinity of intersection of multiple grains in the present simulation case. The growth mechanism of the cracks include crack/damage growth at the grain boundaries of different grains (orientations) as well as the interior regions of the grains, finally extending from short local intra-grain cracks to inter-grain polycrystal scale cracks.

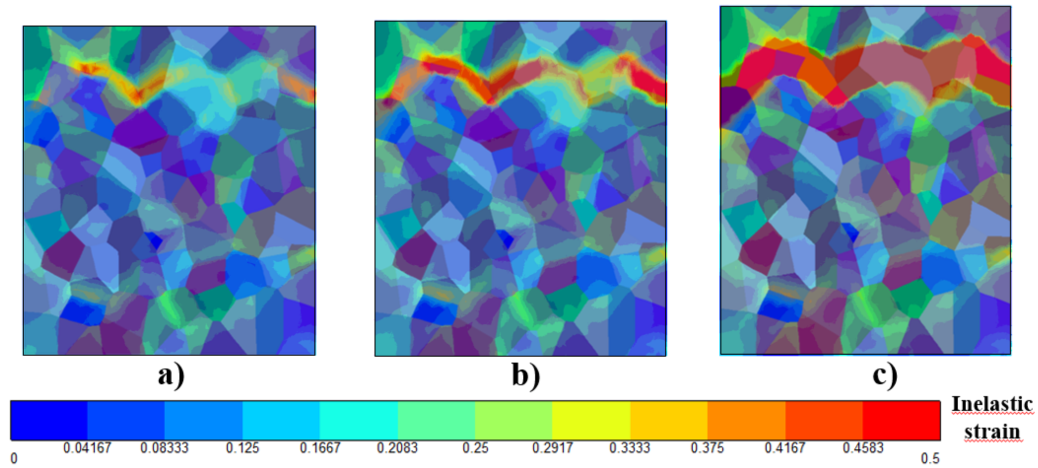

Figure 6: Inelastic strain overlain on the microstructure, at the macroscopic engineering strain of a) 9 %, b) 11 %, c) 16 % during the uniaxial cyclic loading-unloading test.

Utilizing the resulting material model calibration Figure 7 presents the experimental and simulated results of a conventional tensile test until failure. The model agrees well with the measured data with the present parameter set. Table 2 lists the used material parameters. The initial cleavage resistance was set to 1900 MPa after a parametric study. A larger value requires larger softening and coupling factors to better correlate the retarded initiation of softening in the stress-strain curve, while lower value can prematurely initiate damage at lower strains and lead to earlier failure than was experimentally observed. The curve with no active damage shows that the flow stress of the material is higher in the absence of damage and related coupling effects. The isotropic and kinematic viscoplastic response is obtained by way of utilizing cyclic stress-strain curves along with homogenization and self consistent methods, as a part of work presented in [1].

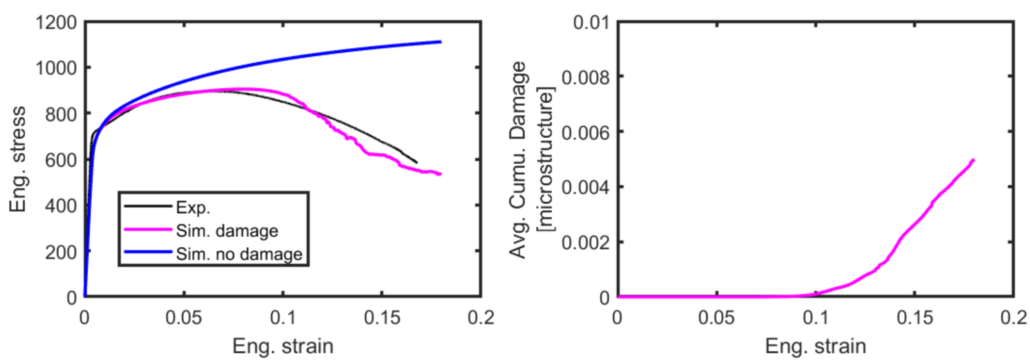

Figure 7: Experimental and simulated tensile test

Table 2: Model parameters for single crystal martensitic Q&T steel.

Parameter	Value	Unit
Elastic constants [30]		
C_{11}	198 000	$[MPa]$
C_{12}	78 125	$[MPa]$
C_{44}	70 700	$[MPa]$
Slip parameters		
τ_0^s	169.0	$[MPa]$
K	169.0	$[MPa.s^{1/n}]$
n	50.0	-
b	19.0	-
Q	37.0	$[MPa]$
C	2000.0	$[MPa]$
D	200.0	$[MPa]$
h_1	1.3	-
h_2	1.0	-
h_3	1.05	-
h_4	1.15	-
h_5	1.1025	-
h_6	1.3	-
h_7	1.4950	-
h_8	1.0	-
Damage parameters		
Y_c^s	1900.0	$[MPa]$
Y_1^s	1900.0	$[MPa]$
Y_2^s	1900.0	$[MPa]$
K_d	5.0	$[MPa.s^{1/n}]$
n_d	2.0	-
H	-1750	$[MPa]$
β	0.265	-

3.3. Strain localization and damage in lath martensite

Figure 8 shows stress-strain curve with damage accumulation for the lath martensitic microstructure in Figure 1c subjected to uniaxial tension. The simulation reproduces a similar strain hardening phase up to about 9-10 % of strain, that was for observed for the polycrystalline microstructure with prior austenite grains only in Figure 6. However, a radical accumulation of damage occurs when axial strain increases, contributing strongly on material's softening. Figure 9 represents equivalent stress contours and inelastic strain distribution in the microstructure at three strain levels.

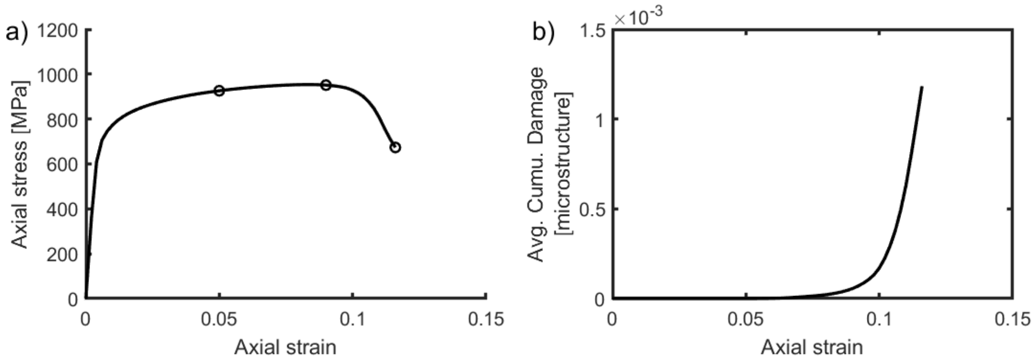

Figure 8: a) Stress-strain curve of lath martensitic microstructure, and b) cumulative damage during applied tensile loading over the entire microstructure.

Stress concentrations are observed in respective different hard and soft orientations within the polycrystalline fine lath martensite. Strain hardening increases the overall strength of the microstructure RVE. At first with 5% of axial strain, local strains are accommodated in favorable sites, but the intensity of straining remains relatively low. However, when overall strain of the microstructure increases, extensive strain localization tends to overcome strain hardening effects and revert to localized strain softening. Strain localization is a driving force for damage that further accumulates plasticity, which finally leads to distinctive local decrease in flow stress and identifiable crack path forms, that is visible in Figure 9a,f. The crack path has evolved to a point, where further restricting boundaries are required to inhibit its growth, and a transition from micro-cracking to short crack growth could be interpreted as consequence, i.e., from submicron size to tens of microns size in the case of the presently studied microstructure.

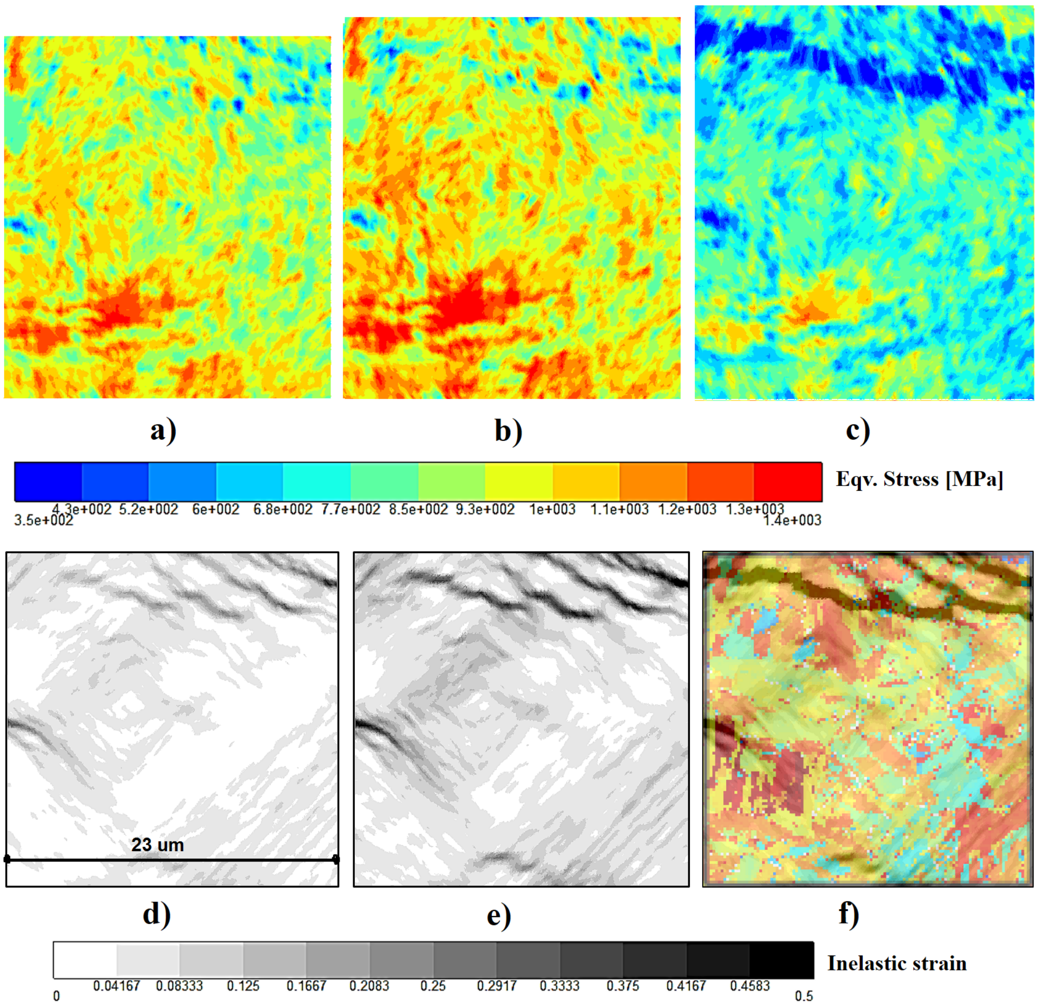

Figure 9: Equivalent stress contours a)-c), and inelastic strain plotted over undeformed shape d)-f) of lath martensite microstructure at different axial strains, 0.05, 0.08 and 0.116, respectively.

3.4. Fatigue application

The effect of damage in cyclic conditions is key aspect in order to capture damage nucleation and crack growth under low, high and very high cycle fatigue. Figure 10a,b shows cyclic stress-strain loops for plasticity-only and plasticity-damage cases. The stress-strain curves are generated by averaging over all of the elements in the full field microstructural mesh, which thus involves elements beyond damaged sites only. A large absolute strain amplitude of $\Delta\varepsilon = 2\%$ was chosen to accelerate strain localization and damage evolution.

A typical cyclic isotropic-kinematic hardening behavior is observed in the absence of damage and related self-softening of the material. Figure 10b shows the softening and effect of damage in the hysteresis. During a phase when plasticity prevails, i.e., damage is not present, the material experiences strain hardening. This phase is similar to the Lemaitre-type loading-unloading experiments and simulations in Figure 5 before cyclic softening and damage effects become relevant. The following damage phase agitates notable softening in the stress-strain loops. This is further pronounced by the tensile-compression asymmetry of the model, with lower flow stress in tension and higher absolute flow stress in compression with a character to introduce apparent hardening behavior towards higher compressive strain. The softening itself is more limited when micro-cracking (damage initiation) is dominant. However, the high strain amplitude of the simulation quickly increases the effect of damage, resulting in the observed dramatic softening of the material within two complete cycles.

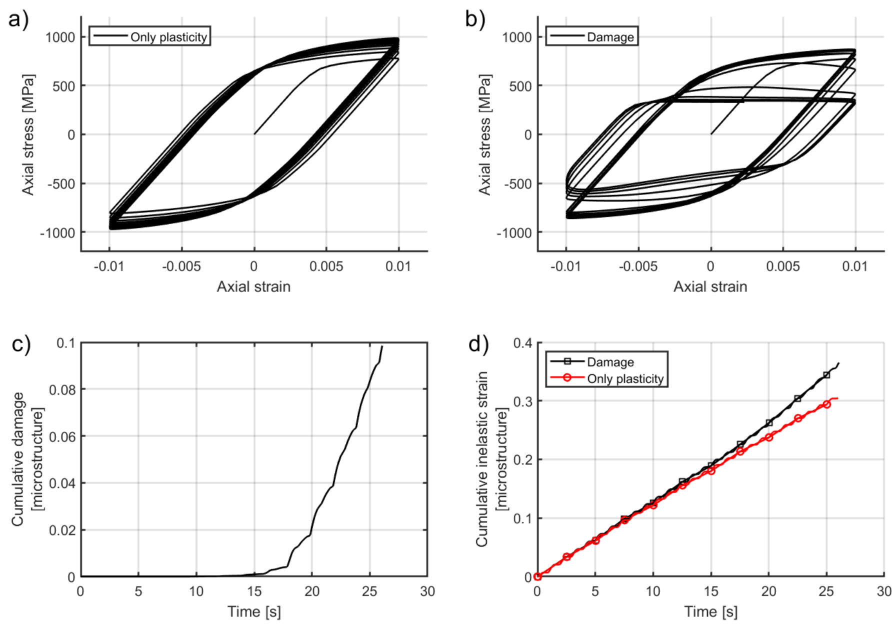

Figure 10: Simulated cyclic mechanical response of the model, stress-strain loops for a) plasticity-only case, b) damage case, and c) cumulative damage for damage case, d) cumulative inelastic strain for both plasticity-only and damage cases. Model is strain controlled with a loading ratio (R) of -1 (fully reversed loading).

The material's flow stress in tension after effective crack growth (damage) in the microstructure is largely restricted by the strain localization and crack opening flow of the damaged regions. After repeated opening-closing sequences, the material has diminishing small resistance against crack opening as already visualized in Figure 2. However, the regions that are only partially damaged and can further inhabit plasticity and damage, or regions with non-opened cracks, still carry out resistance against deformation. These contributions lead to a stable 300-350 MPa flow resistance also at tensile axial strains over the whole microstructure. In addition, a residual strength for slip resistance of 5 % of the initial slip resistance in highly damaged conditions was assumed for numerical stability, i.e., $\tau^s_{res} = max(0.05 \cdot \tau_0, \tau^s)$.

Figure 11b shows how compressive axial strains promote crack closure. However, a crucial observation can be made, the crack closure does not either take place immediately or completely after load reversal to compression. At local scale, some regions of the microstructure can undergo crack closure, but other regions remain partially open and operate as regions with very small flow stress until cracks become closed. This phenomenon causes a hardening effect in the flow stress observed in Figure 10b when more and more cracks close with the increasing compressive axial strain towards 1 %.

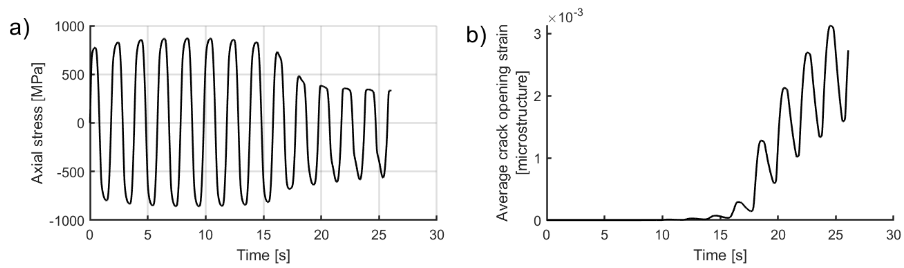

Figure 11: a) Cyclic stress response of the model, and b) average opening strain over the whole microstructure of all cleavage systems as a function of time.

Figure 12a compares accumulation of inelastic strain for plasticity-only and plasticity-damage cases. Strain localization precedes the damage initiation and damage dominant behavior of the steel microstructure. It is expected that the microstructural features drive the strain localization, typically triple points and loading wise soft orientations in the present case. The extent of plastic localization depends much on whether material model can promote local softening through cyclic softening and microdamage.

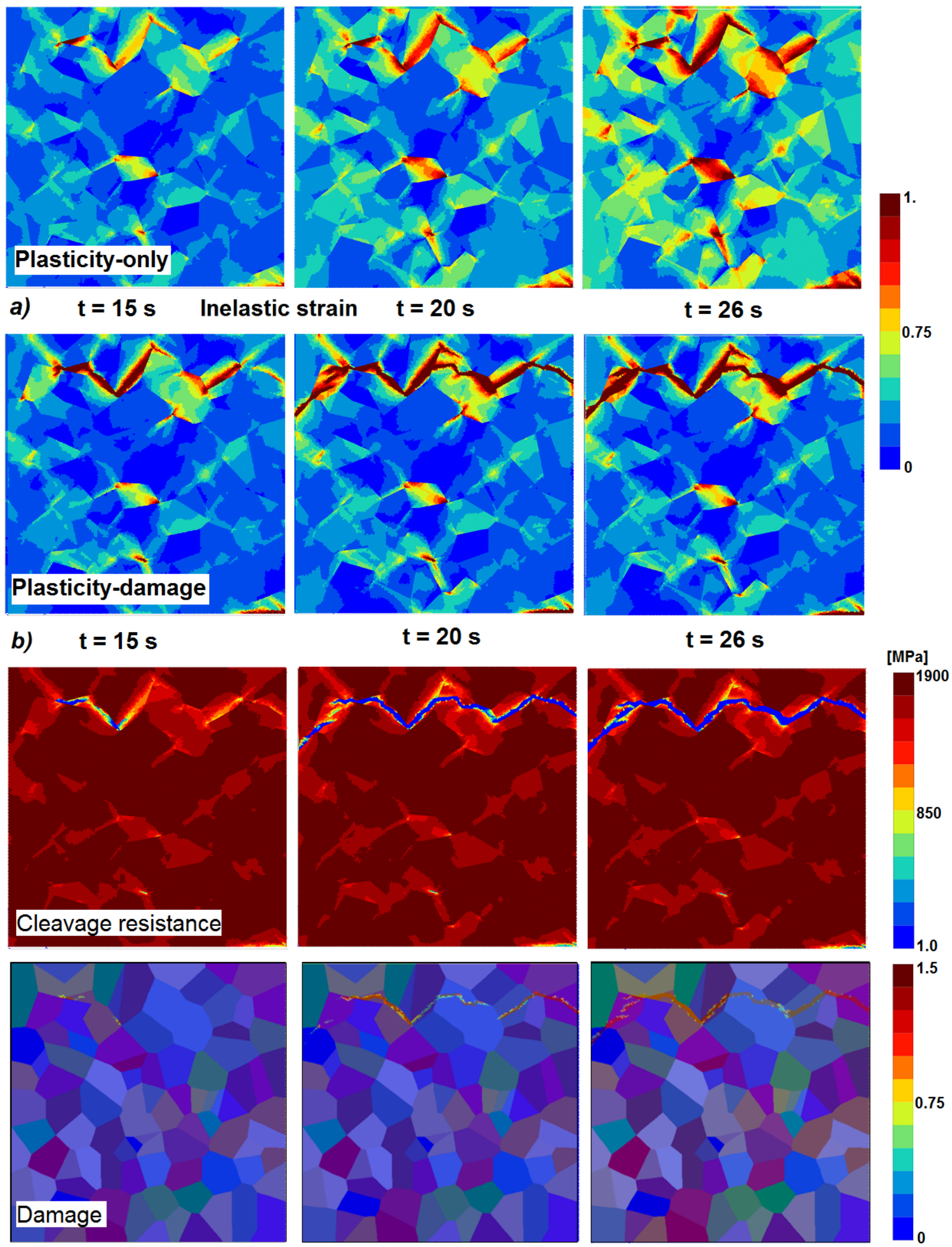

Figure 12: a) Inelastic strain accumulation at different time steps for plasticity-only and plasticity-damage cases, b) cleavage resistance and cumulative damage strain at different time steps.

Plasticity-only case distributes inelastic strain in various regions in the studied RVE, while plasticity-damage case has the capability to drastically sharpen localization, resulting in shear band type of failure zone. Some mesh dependency is expected in the width of the band because of the absence of regularization damage term, as already pointed out with respect to model derivation. Nevertheless, the probability to nucleate crack opening in the plasticity rich zones, whether being narrow or wide, is increasing quickly as a function of decreasing crack opening cleavage resistance shown in Figure 12b. One can use the model to indicate that the material has completely failed at the point where resistance against damage is vanishing small, that was presently chosen to a threshold value of 1 MPa.

4. Discussion

The extension of the introduced micromechanical damage concept to crystal plasticity modeling of plastic slip enabled the coupling between deformation and cleavage type measure of microstructure scale damage. The importance of strain localization preceding material failure in martensitic steels can be investigated in arbitrary loading conditions because of the finite strain implementation of the present model, including the concept's capabilities to capture deformation and failure processes quite generally in polycrystalline microstructures. If follows that the damage path is much dictated by the following strain localization bands, as shown in Figure 12, as is expected. The susceptibility of the material to invoke strain localization, thus, has a significant role in terms of developing damage in the first place, and even more importantly in the transition from micro-cracking to microstructurally short crack state and finally to long more microstructure insensitive crack formation. The progression of this micromechanism ultimately defining the material's performance against failure and also links micromechanics and conventional fracture mechanics.

The model behavior can be adjusted to represent brittle failure character such as could be expected from untempered martensite or even to direct fracture mechanical analyses. Alternatively, large local plastic strains can be allowed for pronounced plasticity driven damage process, e.g., such as those of tempered martensite steel grades. The effectiveness of plasticity-damage coupling and representation of the relationship between micro-cracking and local softening behavior of the material expand the usability of the model, as shown in Figures 3 and 4.

In the view of understanding fundamental reasons for failure during large deformations, complexity of the microstructure has a relevance in the stress concentrations and strain localization in polycrystalline materials. Present work focused on two different cases: a simplified prior austenite based microstructure and SEM imaging based microstructure. Deformation behavior suggests that the strain build-up does not always lead to formation of large individual (short) cracks before further strain localization takes place. Several strain localization zones and thus several susceptible micro-cracking sites can contribute to the formation of crack network. This was the case and typical for both of the investigated microstructure types, as also observed in [1, 10] which also focus on evolution of damage in Q&T steels under comparable loading conditions. Long range effects were observed in Figure 6, where several intra-grain or grain boundary character (near grain boundaries) related micro-defects joined together to form a microstructurally short crack and transition towards a longer crack several PAGs in size. A short range variant of the crack nucleation process was presented in Figure 9. Multiple strain localization sites within 2-5 μm of each other first evolved individually before large macroscopic strain promoted coincidence of the maturing microcracks to form a more extensive crack spanning the entire computational domain. Recently, Chatterjee et al. [29] observed that shear localization has a major role in preceding crack formation. They also noted that the growth of the cracks are inhibited most effectively by block boundaries, while prior austenite and packet boundaries have slightly lesser role in the studied martensitic steel grade. The numerical observations on martensitic microstructure in the current study agrees well with the failure process of their experiments. Further simulations of a number of different discrete martensitic microstructures at different loading conditions could even better validate the model capabilities as well as allow the virtual design of martensitic microstructure to combat damage at loading conditions.

The modeling of fatigue crack growth is a special topic that deserves much attention due to the associated engineering importance. The present work contributes to this field by employing the introduced and calibrated crystal plasticity and damage models as well as the crack closure concept to high strength Q&T steels. An analysis of cyclic loading fatigue case, in Figures 10-12, showed that the model has not only promising features in nucleating and growing cracks (damage) within discrete microstructures, but also the capability to suppress crack growth under tension-compression reverted deformation conditions. Furthermore, with increasing amount of cycles, plasticity and damage, the asymmetric flow stress behavior was demonstrated by the model, a feature considered relevant for assessing defect evolution under cyclic loading in complex microstructures. One origin for this behavior arises from the fact that complete crack closure does not necessarily take place even in fully inverted strain controlled deformation conditions. A present shortcoming of the model is that shear damage was not allowed further take place when the crack is in closed state due to uncertainties in the frictional behavior and contact conditions. In fatigue conditions considering more multiaxial modes of loading, it may have a non-diminishable role and remains an open further point of study.

Size scaling of plasticity and regularization of the damage are not addressed in the present context. Previous papers [25, 24] have suggested formulation of microdamage variable in small deformation framework to control the diffusion of damage in finite element based approaches, with a successful almost complete removal of mesh dependency. An alternative model based on reduced micromorphic formulation has been suggested for ductile damage for FCC materials utilizing Gurson-type of a damage model in [26]. Its finite strain basis enlarges the usability of the model to extreme loading conditions, whereas size scaling is achieved with a cumulative microplasticity extension. They noted that despite microdamage regularization is not directly implemented, as in ref. [24], the plasticity driven damage is also regularized by size dependent plasticity model. In more brittle behavior case, the microdamage approach could provide even better regularization due to less interaction with plasticity. However, as the present model and its related model parameterization are strongly coupled with plasticity, it could become more attractive to simply involve microplasticity driven length scale dependency in the present plasticity model, as suggested in ref. [26]. This strategy may sufficiently provide damage regularization and could remain computationally efficient because of only one added degree of freedom to the formulation. This, however, is considered beyond the scope of this work and a topic for following studies. Another topic of great importance from the material perspective is to address microstructure scale defects such as nonmetallic inclusions, the work which was initiated by present authors in Frondelius et al. [1].

5. Conclusions

A micromechanical approach based on crystal plasticity was used to investigate the strain localization and damage behavior of high strength Q&T

steel under monotonic and cyclic loading conditions. A model coupling plasticity and damage was formulated in a finite strains framework for crystalline BCC materials. The results of this work can be concluded as follows:

- A parametric study on the effect of model parameters was performed, producing a view on the range of feasible material types that could be undertaken by the model. It revealed that the plasticity-damage model can represent characteristics found on brittle and more ductile BCC materials. A model parametrization technique was suggested and utilized for a martensitic Q&T steel grade with a Lemaitre-type tensile loading-unloading experiments using a full field polycrystalline microstructural model. The model could well reproduce the stress-strain behavior and the failure process of the material.

- Model capabilities were investigated with polycrystalline microstructures under severe deformation conditions, including cyclic deformation conditions relevant in fatigue. Plasticity driven damage growth can be simulated with the model from micro-crack evolution over to short crack state progressing from intra-grain to inter-grain and further, irrespective of the complexity of the computational microstructure. This feature opens many opportunities for investigating failure performance of martensitic steels, whenever short crack nucleation and growth control the long crack based failure process.

- Restrictions and improvements of the model related to size dependencies of plasticity and damage regularization are possible to overcome and achievable through modifications in the modeling framework by making use of, e.g., the reduced micromorphic extension.

Acknowledgement

Dr. Andrew Roiko and Tommi Seppanen are gratefully acknowledged for conducting the mechanical experiments. Prof. Samuel Forest is acknowledged for valuable discussions related to the model framework. Finally, the authors would like to acknowledge the financial support of Business Finland (former Tekes) in the form of a research project WIMMA Dnro 1566/31/2015.

Data availability

The raw/processed data required to reproduce these findings cannot be shared at this time as the data also forms part of an ongoing study.

References

References

[1] T. Frondelius, A. Mäntyä, J. Vaara, J. Könnö, T. Andersson, M. Lindroos, T. Verho, A. Laukkanen, Micromechanical modeling of the role of inclusions in high cycle fatigue damage initiation and short crack growth, in: CAASE18 The Conference on Advancing Analysis & Simulation in Engineering, Nafems, 2018.

[2] T. Frondelius, H. Tienhaara, M. Haataja, History of structural analysis & dynamics of Wärtsilä medium speed engines, Rakenteiden Mekaniikka 51 (2018) 1–31.

[3] Y. Murakami, M. Endo, Effects of defects, inclusions and inhomogeneities on fatigue strength, International journal of fatigue 16 (1994) 163–182.

[4] Y. Murakami, Metal fatigue: effects of small defects and nonmetallic inclusions, Elsevier, 2002.

[5] M. D. Sangid, The physics of fatigue crack initiation, International journal of fatigue 57 (2013) 58–72.

[6] M. D. Sangid, H. J. Maier, H. Sehitoglu, A physically based fatigue model for prediction of crack initiation from persistent slip bands in polycrystals, Acta Materialia 59 (2011) 328–341.

[7] M. D. Sangid, G. J. Pataky, H. Sehitoglu, R. G. Rateick, T. Niendorf, H. J. Maier, Superior fatigue crack growth resistance, irreversibility, and fatigue crack growth–microstructure relationship of nanocrystalline alloys, Acta Materialia 59 (2011) 7340–7355.

[8] A. Pineau, S. Forest, Effects of inclusions on the very high cycle fatigue behaviour of steels, Fatigue & Fracture of Engineering Materials & Structures 40 (2017) 1694–1707.

[9] H. Proudhon, J. Li, F. Wang, A. Roos, V. Chiaruttini, S. Forest, 3d simulation of short fatigue crack propagation by finite element crystal plasticity and remeshing, International Journal of Fatigue 82 (2016) 238 – 246.

[10] A. Laukkanen, M. Lindroos, T. Andersson, T. Verho, T. Pinomaa, Micromechanical modeling of failure behavior of metallic materials, Rakenteiden Mekaniikka 50 (2017) 271–274.

[11] D.-F. Li, R. A. Barrett, P. E. O'Donoghue, N. P. O'Dowd, S. B. Leen, A multi-scale crystal plasticity model for cyclic plasticity and low-cycle fatigue in a precipitate-strengthened steel at elevated temperature, Journal of the Mechanics and Physics of Solids 101 (2017) 44 – 62.

[12] Y. Guan, B. Chen, J. Zou, T. B. Britton, J. Jiang, F. P. Dunne, Crystal plasticity modelling and hr-dic measurement of slip activation and strain localization in single and oligo-crystal ni alloys under fatigue, International Journal of Plasticity 88 (2017) 70 – 88.

[13] F. Bridier, D. L. Mcdowell, P. Villechaise, J. Mendez, Crystal plasticity modeling of slip activity in ti–6al–4v under high cycle fatigue loading, International Journal of Plasticity 25 (2009) 1066–1082.

[14] S. Suresh, Near-threshold fatigue crack propagation: a perspective on the role of crack closure, The Metallurgical Society of AIME, Warrendale, PA, 1984 (1984).

[15] S. Pommier, C. Prioul, P. Bompard, Influence of a negative r ratio on the creep-fatigue behaviour of the n18 nickel base superalloy, Fatigue & Fracture of Engineering Materials & Structures 20 (1997) 93–107.

[16] F. Silva, Crack closure inadequacy at negative stress ratios, International journal of fatigue 26 (2004) 241–252.

[17] F. Silva, Fatigue crack propagation after overloading and underloading at negative stress ratios, International Journal of Fatigue 29 (2007) 1757–1771.

[18] J. Vaara, A. Mäntylä, T. Frondelius, Brief review on high-cycle fatigue with focus on non-metallic inclusions and forming, Rakenteiden Mekaniikka 50 (2017) 146–152.

[19] A. Laukkanen, T. Pinomaa, K. Holmberg, T. Andersson, Effective interface model for design and tailoring of WC–Co microstructures, Powder Metallurgy 59 (2016) 20–30.

[20] K. Holmberg, A. Laukkanen, E. Turunen, T. Laitinen, Wear resistance optimisation of composite coatings by computational microstructural modelling, Surface and Coatings Technology 247 (2014) 1–13.

[21] K. Holmberg, A. Laukkanen, A. Ghabchi, M. Rombouts, E. Turunen, R. Waudby, T. Suhonen, K. Valtonen, E. Sarlin, Computational modelling based wear resistance analysis of thick composite coatings, Tribology International 72 (2014) 13–30.

[22] H. Proudhon, J. Li, W. Ludvig, A. Roos, S. Forest, Simulation of short fatigue crack propagation in a 3d experimental microstructure, Advanced Engineering Materials 19 (2017) 1–9.

[23] Lemaitre Jean, A Continuous Damage Mechanics Model for Ductile Fracture, Journal of Engineering Materials and Technology 107 (1985) 83–89. 10.1115/1.3225775.

[24] O. Aslan, N. Cordero, A. Gaubert, S. Forest, Micromorphic approach to single crystal plasticity and damage, International Journal of Engineering Science 49 (2011) 1311–1325.

[25] P. A. Sabnis, S. Forest, J. Cormier, Microdamage modelling of crack initiation and propagation in fcc single crystals under complex loading conditions, Computer Methods in Applied Mechanics and Engineering 312 (2016) 468–491.

[26] C. Ling, S. Forest, J. Besson, B. Tanguy, F. Latourte, A reduced micromorphic single crystal plasticity model at finite deformations. application to strain localization and void growth in ductile metals, International Journal of Solids and Structures 134 (2018) 43–69.

[27] T. Hoc, S. Forest, Polycrystal modelling of if-ti steel under complex loading path, International Journal of Plasticity 17 (2001) 65–85.

[28] A. Ghost, S. Kundu, D. Chakrabarti, Effect of crystallographic texture on the cleavage fracture mechanism and effective grain size of ferritic steel, Scripta Materialia 81 (2018) 8–11.

[29] A. Chatterjee, A. Ghosh, A. Moitra, A. Bhaduri, R. Mitra, D. Chakrabarti, Role of hierarchical martensitic microstructure on localized deformation and fracture of 9cr-1mo steel under impact loading at different temperatures, International Journal of Plasticity 104 (2018) 104–133.

[30] N. Osipov, Génération et calcul de microstructures bainitiques, approche locale intragranulaire de la ruptur, MINES ParisTech, 2007.